Estimation of Multi-Frequency, Multi-Incidence and Multi-Polarization Backscattering Coefficients over Bare Agricultural Soil Using Statistical Algorithms

Rémy Fieuzal, Frédéric Baup

applied sciences

MDPI

Article

Estimation of Multi-Frequency, Multi-Incidence and Multi-Polarization Backscattering Coefficients over Bare Agricultural Soil Using Statistical Algorithms

Rémy Fieuzal [1,*] and Frédéric Baup [1,2]

[1] Centre d'Études Spatiales de la BIOsphère (CESBIO), Université de Toulouse, CNES/CNRS/INRAE/IRD/UT3, 18 Avenue Edouard Belin, 31401 Toulouse, France
[2] IUT Paul Sabatier, 24 Rue d'Embaquès, 32000 Auch, France
* Correspondence: remy.fieuzal@univ-tlse3.fr; Tel.: +33-561-556-484

Abstract: In the last decade, many SAR missions have been launched to reinforce the all-weather observation capacity of the Earth. The precise modeling of radar signals becomes crucial in order to translate them into essential biophysical parameters for the management of natural resources (water, biomass and energy). The objective of this study was to demonstrate the capabilities of two statistical algorithms (i.e., multiple linear regression (MLR) and random forest (RF)) to accurately simulate the backscattering coefficients observed over bare agricultural soil surfaces. This study was based on satellite and ground data collected on bare soil surfaces over an agricultural region located in southwestern France near Toulouse. Multi-configuration backscattering coefficients were acquired by TerraSAR-X and Radarsat-2 in the X- and C-bands, in co-(abbreviated σ^0_{HH} and σ^0_{VV}) and cross-polarization states (abbreviated σ^0_{HV} and σ^0_{VH}) and at incidence angles ranging from 24° to 53°. Models were independently calibrated and validated using a ground dataset covering a wide range of soil conditions, including the topsoil moisture (range: 2.4–35.3%), root-mean-square height (range: 0.5–7.9cm) and clay fraction (range: 9–58%). Higher-magnitude correlations (r) and lower errors (RMSE) were obtained when using RF (r values ranging from 0.69 to 0.86 and RMSE from 1.95 to 1.00 dB, depending on the considered signal configuration) compared to MLR (r values ranging from 0.58 to 0.77 and RMSE from 2.22 to 1.24 dB). Both surpass the performance presented in previous studies based on either empirical, semi-empirical or physical models. In the linear approach, the information is mainly provided by the surface moisture and the angle of incidence (especially in the case of co-polarized signals, regardless of the frequency), while the influence of roughness or texture becomes significant for cross-polarized signals in the C-band. On the contrary, all the surface descriptors contribute in the approach based on RF. In future work, the use of the RF algorithm developed in this paper should improve the estimation of soil parameters.

Keywords: bare soil; topsoil moisture; surface roughness; soil texture; microwave; TerraSAR-X; Radarsat-2; multiple linear regression; random forest

Citation: Fieuzal, R.; Baup, F. Estimation of Multi-Frequency, Multi-Incidence and Multi-Polarization Backscattering Coefficients over Bare Agricultural Soil Using Statistical Algorithms. *Appl. Sci.* **2023**, *13*, 4893. https://doi.org/10.3390/app13084893

Academic Editors: Samuel Adelabu, Romano Lottering and Kabir Peerbhay

Received: 27 February 2023
Revised: 1 April 2023
Accepted: 10 April 2023
Published: 13 April 2023

1. Introduction

During the last decade, many SAR missions (SENTINEL-1A/B, SAOCOM, ICEYE, DENALI, SEOSAR…) have been added to the well-known pioneer missions (ERS, Radarsat-2, RCM, Envisat, TerraSAR-X, Tandem-X, COSMO-SkyMed, Kompsat-5…). Consequently, access to a wide range of images acquired with different configurations has been facilitated, which reinforces the need to develop radar backscatter models capable of simulating the delivered signals in order to estimate the biophysical parameters of the surface. The analysis and interpretation of SAR signals remain challenging and can lead to conflicting explanations for our observations of the environment. It is recognized that backscatter coefficients are sensitive to multiple changes in surface conditions and that the same value may be the result of extremely different vegetation or soil conditions due to compensation

and the equifinality effects of surface and radar antenna parameters. For example, a dry bare soil could have the same backscatter coefficient value as a well-developed wheat field depending on surface conditions (soil moisture, vegetation water content, roughness, plant density...) or antenna geometry (frequency, incidence angle, polarization...) [1,2]. To better understand these effects of equifinality and to better differentiate the contributions related to the variation in surface states, numerous studies have treated these two entities separately [3,4].

In periods of bare soil, surface soil moisture, roughness and texture have been identified as variables whose dynamics influence the intensity of backscattering [5–9]. These three surface descriptors thus constitute explanatory variables common to many approaches, with the models being based on relationships determined from in situ datasets (semi-empirical models [10–12]) or on a physical description of backscatter processes (mechanistic models [13–18]). In remote sensing, most models used for thematic applications are semi-empirical or statistical because of their ease of application for large landscapes. Physical models are currently used for theoretical surface conditions [19–23], where the required soil characterization or computation time is not feasible at the scale of a territory covered by a satellite image. They are fundamental to better understanding the different contributors of the backscattered signal but remain limited to specific cases (a very well-known plot or a simulated theoretical plot, for example), where scientists have total control over the surface conditions. With the objective of applying the method over large agricultural surfaces, we will not consider these physical models and we will concentrate on the most used models in applied remote sensing.

Approaches based on empirical, semi-empirical or statistical models have varying levels of complexity and are based on a different number of surface descriptors. Nevertheless, these modeling approaches offer limited performance regardless of the tested sensor configurations, particularly for applications aimed at monitoring agricultural surfaces [24]. In this context, more recent studies have proposed different ways to modify models (i.e., by recalibration, taking into account biases or even adding empirical relationships to physical models) and attempted to improve the description of backscatter processes by taking better account of surface variables [24–30]. As models often present limitations in the representation of surface roughness, modifications were proposed that aimed at improving the formalism and extending the field of validity [24] in order to make it possible to apply the approaches to the high values observed in the agricultural context [31–33]. These modeling efforts have obviously been accompanied by a reduction in dispersion and bias, resulting in an overall increase in performance. Nevertheless, the correlation levels obtained between the satellite-derived backscattering coefficients and the predicted values are often mixed (with values between 0.05 and 0.85, depending on the modeling approach and satellite configuration), as are the errors made in the estimation of backscattering coefficients (with values close to 1 dB in rare cases).

Statistical approaches present a tangible alternative to those used in previous studies, offering precise performance even when processes are complex and multifactorial. Often used with SAR data for classification purposes [34–37], statistical algorithms can also constitute one of the links in the chain of methods to provide estimates of surface moisture [38–43], roughness [38,44,45] or texture [46]. In most of these approaches, the statistical algorithm is considered an inversion tool, trained on a synthetic database derived from the models discussed above [38–42]. The limits of the representativeness of the models are then reflected in the estimation of the surface parameters, as evidenced by the performance levels. Only a few studies have avoided the use of backscattering models by training and validating the statistical approach directly on an in situ dataset [47–51].

In this context, the originality of our study is the estimation of backscattering coefficients using two statistical approaches, multiple linear regression (MLR) and random forest (RF), to simulate the backscatter coefficients acquired in the X- and C-bands in HH, VV and VH polarization states in bare ground agricultural areas. This paper is structured as follows: First, the study site, ground measurements and satellite data are described (Section 2).

The methodology description presents the two statistical algorithms and steps required to estimate microwave signals and to analyze the importance of the input variables (Section 3). The results are analyzed considering the overall performance and the importance of the explanatory descriptors. The main findings are discussed and compared with previous studies concerning the modeling of backscattering coefficients or signal analysis (Section 4).

2. Materials

2.1. Study Area

The study area (defined as the super site in Figure 1) is located in southwestern France in the Midi-Pyrénées region, covering a surface area of approximately 420 km^2. The landscape is characteristic of 'Garonne's terraces', with the presence of hills and alluvial plains. The surveyed plots (37) are flat in the east (with slopes mostly less than 1°) and more marked in the west (with slopes nearing an average of 4.5°). They have very different shapes and sizes, with areas between 2 and 38 hectares (11 hectares on average over the area). The study site is subject to a temperate climate, characterized by a marked seasonality. During the year 2010, the annual cumulative rainfall exceeded 600 mm, with high variability between months (e.g., 20% of annual rainfall recorded in May). Temperatures varied from a mean of 3.5 °C in January to 22 °C in July. The study area is highly anthropized, with 90% of the area dedicated to agriculture and 57% of the area allocated to seasonal crops.

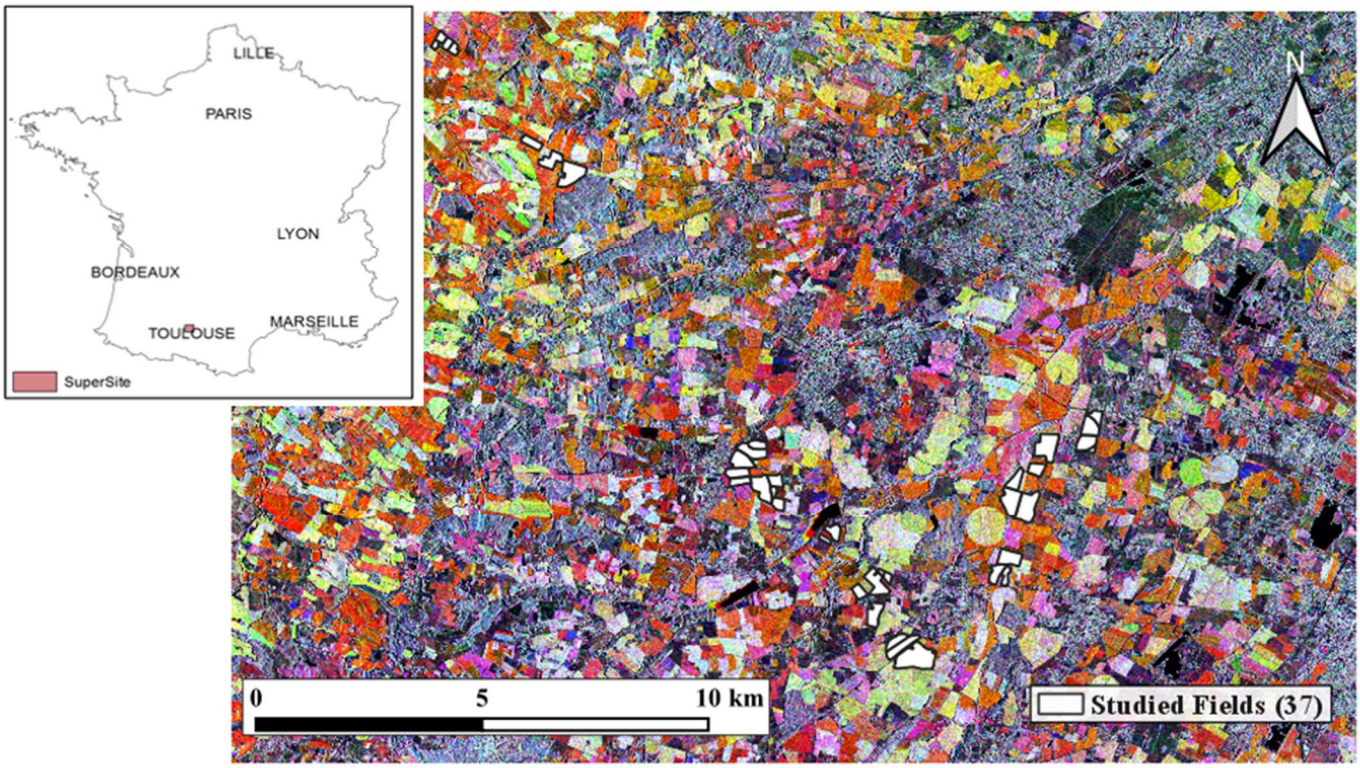

Figure 1. Location of the study site (super site) in southwestern France. The network of the 37 surveyed fields (white polygons) is superimposed on a color-composed TerraSAR-X image acquired in StripMap mode in HH polarization (red: 23 November 2010; green: 16 August 2010; blue: 20 May 2010).

During the agricultural season, bare soil conditions are mainly observed during spring and autumn, as illustrated in Figure 2. The first period is observed during the months of April and May; the plots dedicated to summer crop cultivation (i.e., maize, soybean or sunflower) are tilled, and different surface states succeed each other until planting. The second period of tillage occurs between the months of October and November, and different roughness levels are then observed, corresponding to the soil preparation before the sowing of winter crops (i.e., wheat and rapeseed), stubble disking or harrowing in order

to manage the crop residues and mold the first centimeters of the plot, or deep plowing to overcome densely packed soils. A network of surveyed plots has thus been determined in order to characterize the strong heterogeneity as well as the important dynamics of the surface variables.

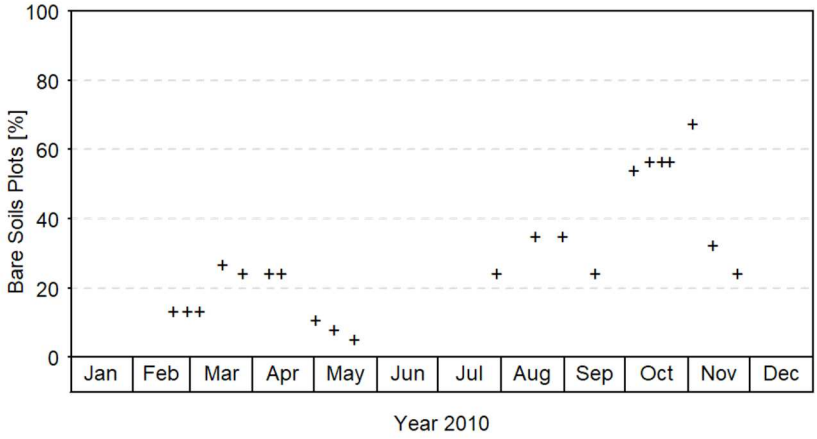

Figure 2. Relative number of bare soil plots (%) during the field campaign.

2.2. In Situ Data

The main characteristics (i.e., dates, range and mean values) of topsoil moisture (TSM), soil texture and surface roughness measurements collected in bare soil conditions are summarized in the Table 1. The protocols and the mean features of the collected soil descriptors are described hereinafter.

Table 1. Overview of the measurements collected on the network of plots. Surface roughness is divided into perpendicular (⊦) and parallel (| |) measurements compared to the row direction.

Soil	Variable	Measurement	Values
Descriptor	**Name (Unit)**	**Date**	**[Min–Max] Mean**
Topsoil Moisture	(% $m^3.m^{-3}$)	20 February 2010	[24.0–32.9] 28.9
		27 February 2010	[20.1–25.2] 23.3
		5 March 2010	[21.2–31.0] 27.0
		16 March 2010	[11.8–23.7] 17.9
		26 March 2010	[11.5–25.6] 20.8
		8 April 2010	[6.7–24.6] 15.9
		14 April 2010	[3.5–18.9] 11.2
		1 May 2010	[25.8–31.2] 28.7
		10 May 2010	[20.0–24.1] 21.8
		20 May 2010	[12.5–15.5] 14.0
		29 July 2010	[7.0–17.0] 11.1
		17 August 2010	[2.7–10.8] 5.9
		30 August 2010	[2.5–6.0] 3.8
		15 September 2010	[2.4–6.4] 4.2
		4 October 2010	[7.0–16.3] 11.2
		12 October 2010	[21.3–31.3] 25.5
		18 October 2010	[9.8–21.9] 14.5
		22 October 2010	[7.7–17.8] 12.1
		2 November 2010	[18.1–29.2] 23.3
		12 November 2010	[22.6–35.3] 26.6
		24 November 2010	[22.0–29.6] 26.3
Soil Texture	Clay (%)	Once during	[9–58] 24
	Silt (%)	the experimental	[22–77] 52
	Sand (%)	period	[4–53] 24

Table 1. *Cont.*

Soil	Variable	Measurement	Values
Descriptor	**Name (Unit)**	**Date**	**[Min–Max] Mean**
Surface Roughness	├ h_{rms} (cm)		[0.6–7.9] 2.2
	├ l_c (cm)	After each	[1.9–18.5] 7.7
	| | h_{rms} (cm)	tillage event	[0.5–5.6] 1.5
	| | l_c (cm)		[1.1–14.9] 4.4

2.2.1. Topsoil Moisture

The spatial variability in the topsoil moisture (0–5 cm) was measured quasi-synchronously with satellite acquisitions (i.e., time differences between in situ measurements and satellite acquisitions of less than one day for 77% of cases for TerraSAR-X acquisitions and 81% for Radarsat-2) by using portable probes (ML2x from ThetaProbe). The first protocol aims at determining a calibration relationship for the conversion of the probe's signal, delivered in mV, to volumetric moisture expressed in cubic meters of water per cubic meter of soil ($m^3.m^{-3}$) or percentage (%). The sampling method consisted of synchronously performing measurements with the probe and sampling the soil in the same location. The soil sample was used to estimate the volumetric moisture, with the water content of the sample being determined by weight. The sample was weighed, dried for at least 48 h at 105 °C and then weighed again. The resulting calibration function is given by Equation (1) [52]:

$$TSM(\%) = 0.04 \times mV + 0.08 \left(R^2 = 0.75, \text{RMSE} = 4.1\%, \text{n} = 403\right), \quad (1)$$

The monitoring of soil moisture in the study area was then performed using similar portable probes to those used for the calibration step. The measurements were collected every 10 or 20 m along transects ranging from 40 to 640 m (depending on the size of the plot).

The time course of soil moisture measurements collected in bare soil conditions is presented in Figure 3. The average and standard deviation values of topsoil moisture were derived from measurements collected during the 21 dates of observation. The measurements cover a wide range of values, as shown by the average values, which vary between 3.8% (observed during the summer months, after the harvest of the winter crops) and 29.8% (observed during the rainy period in February and May). At the end of the year (in November), the values are comparable to those collected in February (almost 27%). The variability in topsoil moisture values is much more important during the first months of the year (from February to April). The regular measurements of topsoil moisture allow the collection of data in varying conditions (i.e., dry to wet soil), as highlighted by values at the plot spatial scale, ranging from 2.4 to 35.3%.

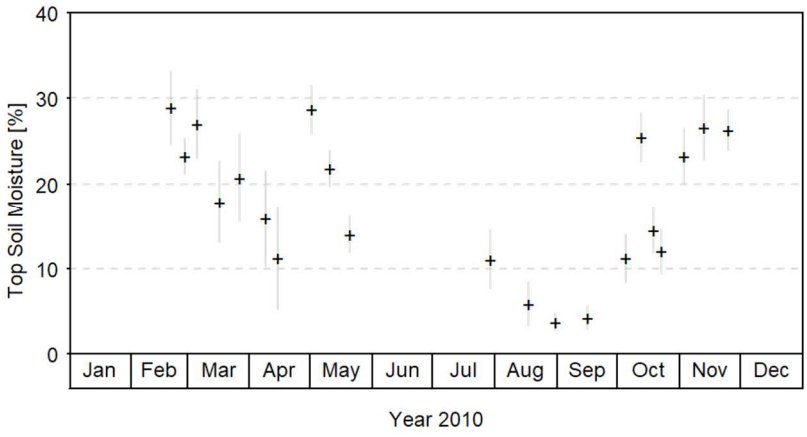

Figure 3. Time course of topsoil moisture (mean (black dots) and standard deviation (in gray) values) collected on the monitored plots with bare soil conditions.

2.2.2. Soil Texture

The samples (146) were collected along the same transects used for the measurements of topsoil moisture. Each measurement 'point' consisted of 16 core samples within a circle with a 15 m diameter and a depth of 25 cm. The number of 'points' measured in each plot ranged from 2 to 8 and is a function of (i) the length of the transect and (ii) the analysis of surface moisture measurements. The plots showing specific soil moisture profiles; namely, a trend or different levels of values along the transect were intentionally oversampled. The 'Lara Europe Analyses' laboratory obtained the fractions of clay, silts, sands and gravels.

The fractions of clay, silt and sand are presented within the United States Department of Agriculture (USDA) classification system (Figure 4). This classification is divided into 12 classes of texture, 7 of which are assigned to the measurements. The samples are mostly in the silty loam class (with 77 samples), followed by loam (20), silty clay loam (16), clay loam (15), clay (10), silty clay (5) and sandy clay loam (3). With fractions between 9 and 58% for clay, between 22 and 77% for silt and between 4 and 53% for sand, the observed contents cover approximately half of the range of each component. On average, the texture is composed of 52% silt and 24% clay and sand, illustrating the dominance of the silt fraction within the study area. Moreover, 95% of samples have a sand content of less than 40%, and more than half of the points have a clay content that does not exceed 20%.

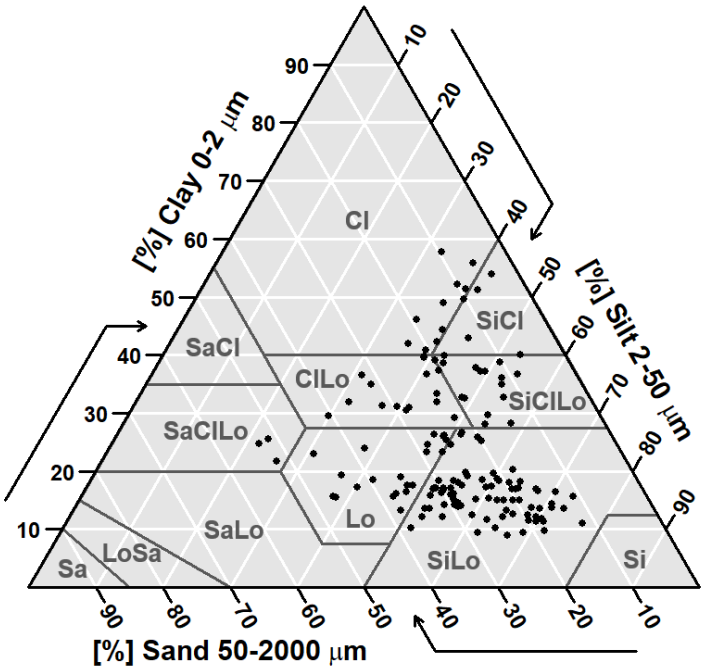

Figure 4. Surface texture measurements (black dots) displayed on the United States Department of Agriculture (USDA) classification system with the following classes: clay (Cl), silty clay (SiCl), sandy clay (SaCl), clay loam (ClLo), silty clay loam (SiClLo), sandy clay loam (SaClLo), loam (Lo), silty loam (SiLo), sandy loam (SaLo), silt (Si), loamy sand (LoSa) and sand (Sa).

2.2.3. Surface Roughness

The surface roughness was measured using a 2 m long needle profilometer after each tillage event. Tillage was either plowed, stubble-disked, harrowed, prepared cloddy or prepared smooth. The profilometer is composed of 201 needles spaced 1 cm apart. These needles replicate the micro-relief of the ground by landing on the surface, and a photograph records the soil profile. For each change in the surface state, two profiles were collected parallel to the direction of the tillage of the plot, and two others were collected perpendicularly.

Pairs of pictures were digitized and associated to obtain 4 m long profiles. The first-order trend was removed to subtract the effect of the local slope due to non-parallelism between the soil and the profilometer. A statistical description of the roughness is provided by the root-mean-square height (h_{rms}). The dependence between two successive points of the roughness profile was estimated through the exponential or Gaussian correlation function, defining a distance for which the correlation between points no longer exists, or the correlation length (l_c).

The values of h_{rms} and l_c, derived from parallel and perpendicular profiles and grouped into four categories according to tillage practices, are presented in Figure 5. The values are highest in the perpendicular direction, as evidenced by the average h_{rms} of 2.2 cm (vs. 1.5 cm in the parallel direction) or l_c of 7.7 cm (vs. 4.4 cm). The 'plowed' surface state presents the highest values of h_{rms} (with averages of 3.4 and 4.4 cm in the parallel and perpendicular directions) and differs from other levels of roughness. It represents 11% of the collected profiles and is associated with high variability, as evidenced by the values of the coefficients of variation between 25 and 45%, depending on the parameter (h_{rms} or l_c) and the direction considered. The 'stubble disked' and 'harrowed' surface states represent, respectively, 14 and 23% of the collected profiles. They are associated with fairly close h_{rms} values, with an average of 1.5 and 1.8 cm in the parallel direction and 2.7 and 2.4 cm in the perpendicular direction. They are therefore difficult to separate, especially as they have high dispersion, with coefficients of variation greater than 30%. The 'prepared' surface states account for more than half of the roughness measurements (25% for the 'cloddy' state and 27% for 'smooth'). They are associated with fairly close h_{rms} values, less than 2 cm on average. The l_c values are more mixed, with greater averages for the 'smooth' state compared to 'cloddy' (with 4.4 vs. 2.5 cm in the parallel direction and 8.5 vs. 6.0 cm in the perpendicular direction).

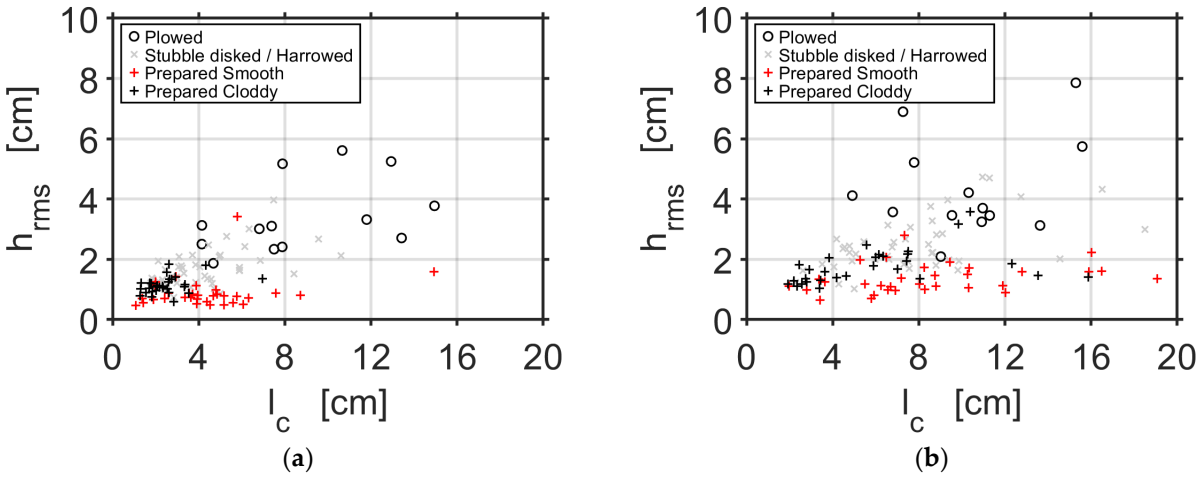

Figure 5. Scatter plot between roughness parameters (root-mean-square height (hrms) and correlation length (lc)) derived from parallel (**a**) and perpendicular (**b**) profiles. Roughness states are grouped into four categories according to soil practices (plowed, stubble-disked, harrowed, prepared cloddy and prepared smooth).

2.3. Microwave Satellite Data

The German and Canadian satellites, namely, TerraSAR-X and Radarsat-2, respectively, provide microwave data. They carry SAR instruments that operate in the X-band (f = 9.65 GHz, λ = 3.1 cm) and in the C-band (f = 5.405 GHz, λ = 5.5 cm). The satellite acquisitions are planned in order to constitute the maximum number of pairs of images presenting the two frequencies in close intervals of time. Throughout the agricultural season, 27 images in the X-band and 21 in the C-band were collected on plots presenting bare soil conditions (Table 2).

Table 2. Mean features of the TerraSAR-X and Radarsat-2 acquisitions.

Mission	Mode	Acquisition Date (mm, dd, yy)	Pass	Incidence Angle (°)	Pixel Size (m)	Polarization States
TS-X	Spotlight	15 March 2010	D	28.7	2	HH
TS-X	Spotlight	14 April 2010	A	32.3	2	HH
TS-X	Spotlight	8 April 2010; 30 April 2010; 29 August 2010	A	45.5	1.75	HH
TS-X	Spotlight	5 March 2010; 21 May 2010; 18 August 2010	D	53.3	1.5	HH
TS-X	StripMap	30 September 2010; 11 September 2010; 22 September 2010 2 November 2010; 13 November 2010; 24 November 2010 21 February 2010; 26 March 2010; 9 May 2010; 20 May 2010 16 August 2010; 29 September 2010; 10 October 2010 21 October 2010; 12 November 2010; 21 November 2010	D	27.3	2.75	HH
TS-X	StripMap	15 September 2010	A	31.8	2.75	HH
TS-X	StripMap	27 February 2010; 31 July 2010	D	41.7	3	HH
RS-C	FQ5	5 March 2010; 24 November 2010	A	24.3	5	Full
RS-C	FQ6	21 October 2010; 14 November 2010	D	25.6	5	Full
RS-C	FQ10	26 February 2010; 15 April 10; 9 May 2010; 30 September 2010	A	30.0	5	Full
RS-C	FQ11	26 March 2010; 17 August 2010	D	31.1	5	Full
RS-C	FQ15	15 March 2010; 8 April 2010; 2 May 2010; 30 August 2010; 17 October 2010	A	35.1	5	Full
RS-C	FQ16	20 May 2010; 31 July 2010; 11 October 2010	D	36.2	5	Full
RS-C	FQ20	3 November 2010	A	39.9	5	Full
RS-C	FQ21	20 February 2010; 16 March 2010	D	40.8	5	Full

TerraSAR-X images are acquired in HH polarization using two beam modes (SpotLight (SL) and StripMap (SM)) and are characterized by a pixel spacing ranging from 1.5 to 3 m [53]. They are mainly acquired at incidence angles of 27.3° and 53.3° (11 and 10 images, respectively), although a third part of the images is associated with intermediate incidence angles (28.7°, 31.8°, 32.3°, 41.7° or 45.5°). Radarsat-2 images are acquired in the full quad-polarization mode (FineQuad-Pol), which provides images in HH, VV, HV and VH polarizations, with a pixel spacing of ~5 m [54]. They are acquired with eight different incidence angles, ranging from 24° to 41°. All radar images were calibrated and geo-referenced using ortho-photos (with a resolution of 50 cm) provided by the French National Geographic Institute [53,55].

3. Methods

The present work addresses the estimation of backscattering coefficients at the spatial scale of the plot. The steps implemented in the estimation of backscattering coefficients are illustrated in the following synopsis (Figure 6). Microwave satellite images are first processed to obtain backscatter coefficients at the plot scale (processing steps described in Section 2.3). The backscattering coefficients are then estimated using the two statistical algorithms described below (i.e., multiple linear regression or random forest). These algorithms were implemented by considering all collected soil measurements, allowing the analysis of variable importance.

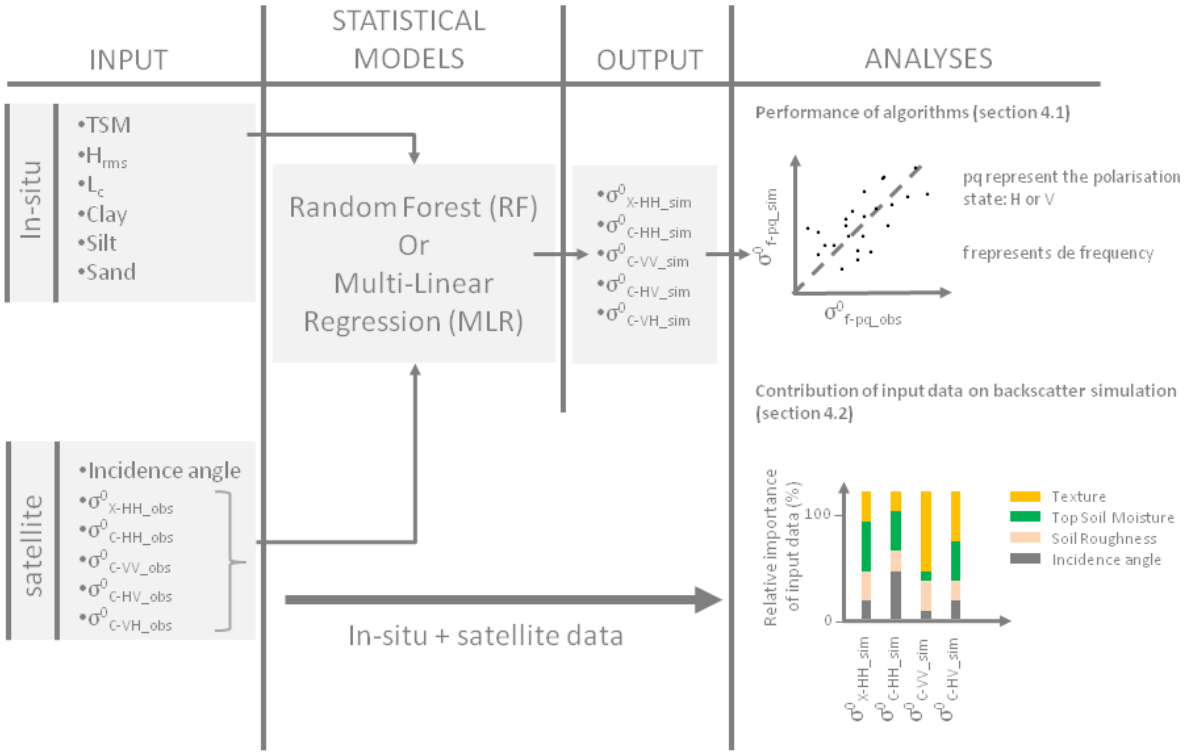

Figure 6. Synopsis of the methodology.

3.1. Multiple Linear Regression

The studies carried out on the interpretation of the dynamics of the backscatter coefficients, as well as on their modeling, showed that the radar signals observed in bare soil conditions depend on several variables. For each of the satellite configurations studied in this paper, multiple linear regression was performed. This method aims at estimating the linear relationship between the backscatter coefficients (variable to be predicted, or Y) and the surface descriptors, classically considered explanatory variables in modeling approaches (explanatory variables, or X_1, X_2, . . . , X_N). The significance of the multiple linear regression coefficients was determined, along with their corresponding p-values. The surface and satellite descriptors were retained in the algorithm when the p-value was below the significance level of 0.05 for a considered explanatory variable (which allows the null hypothesis to be rejected and the hypothesis of a non-zero correlation to be accepted).

3.2. Random Forest

The relationships between surface descriptors and backscatter coefficients may be more complex and non-linear, and the effects between explanatory variables on the dynamics of satellite signals can be combined. In this multifactorial context, an algorithm such as random forest appears to be appropriate [56], particularly when non-linear behaviors exist. Estimates of the target variable are obtained as follows: an ensemble of independent trees is constructed from a subset of bootstrap samples derived from the original dataset and aggregated through the weighted mean of the ensemble of estimates, providing an estimate of the targeted variable. The bootstrap aggregating procedure (also called bagging) provides a number of benefits, including reduced overfitting, the low influence of noise on the data and the high stability of the results. Furthermore, the algorithm provides a measure of the relative importance of the predictive variables, which can be used to rank, to select or to understand the influence of the considered explanatory variables [57].

3.3. Statistical Model Setup and Accuracy Metrics

Regardless of the considered statistical algorithm, the backscattering coefficients were first estimated by considering the following explanatory variables: the incidence angle for the SAR images; the topsoil moisture; the fractions of clay, silt and sand for the texture; and the standard deviation of roughness heights and the autocorrelation length collected in the directions parallel and perpendicular to the tillage orientation for the surface roughness. Regardless of the considered SAR signal configuration, the dataset was randomly divided into a training set and a test set, each containing half of the data. The statistical algorithms were calibrated on the training set and validated on the independent test set, repeating the procedure ten times. The average values of the coefficient of correlation, root-mean-square error and bias were finally derived from the comparison between the observed and estimated values of the backscatter coefficients (Equations (2)–(4)).

$$r = \frac{\mathrm{COV}(o, p)}{\sigma_o \sigma_p}, \tag{2}$$

$$RMSE = \sqrt{\frac{\sum_{i=1}^{n} (p_i - o_i)^2}{n}}, \tag{3}$$

$$Bias = \frac{1}{n} \sum_{i=1}^{n} (p_i - o_i), \tag{4}$$

where n is the number of observed values, o is the observed value, p is the predicted value, COV is the covariance, and σ_o and σ_p are the standard deviations of observed and predicted data, respectively.

The values of the multiple linear regression parameters are summarized in Appendix A for each studied satellite configuration, and the trained random forest models are available by request from the authors or can be downloaded by following the link provided in the section "Supplementary Materials".

4. Results and Discussion

4.1. Overall Performance of the Statistical Approaches

4.1.1. Multi-Incidence Estimates of X-Band Backscattering Coefficients

The values of backscattering coefficients estimated in HH polarization using the MLR or RF algorithm are compared to those derived from the TerraSAR-X images (Figure 7). The independent subsets of samples used for the training and validation phases are distinguished (in gray and black, respectively) and associated with their corresponding statistical indices. Regarding MLR, the estimates of the backscatter coefficients are based on the incidence angle and the topsoil moisture, which are the only explanatory variables among those tested to present p-values lower than 0.05. All surface and satellite descriptors were retained for the RF algorithm. Higher accuracy is observed for estimates based on RF compared to the performance obtained with MLR, as highlighted by the values of correlation of 0.86 and 0.77 (values obtained with the validation subset of samples). A more in-depth analysis of the validation subset shows that backscattering coefficients are estimated without any bias (values close to 0), with a high level of correlation (values greater than 0.75) and with an acceptable level of error (values of RMSE less than 1.3 dB), regardless of the considered statistical algorithm. Such a level of performance surpasses the results obtained in the same study site using Oh's and Dubois' semi-empirical models [10–12,30]. As detailed in the following Section 4.1.3, these performance metrics are also superior to those obtained using a dataset collected at other study sites used to test or to develop modified versions of Oh's and Dubois' models.

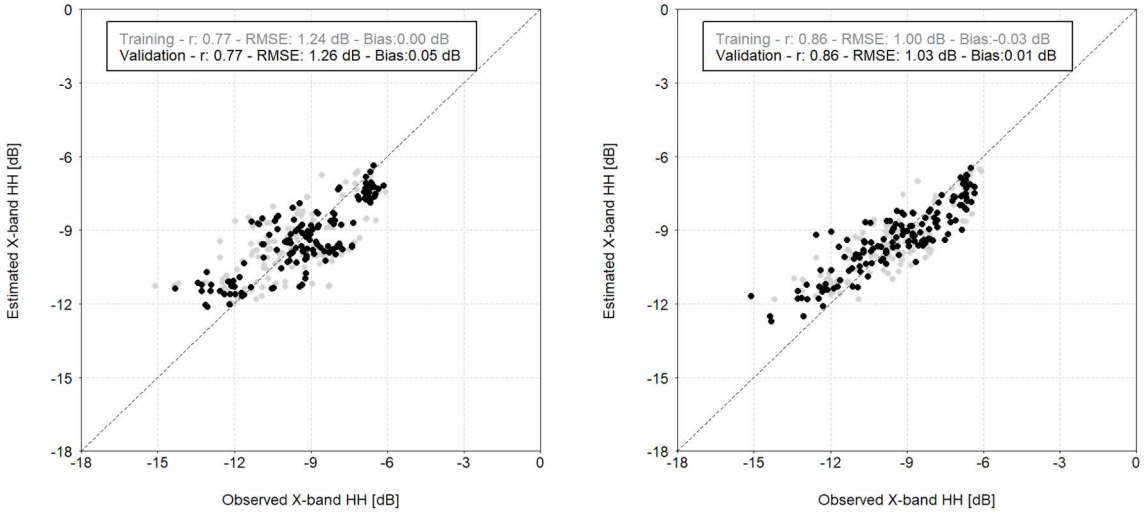

Figure 7. Comparison between simulated and observed backscattering coefficients in the X-band with HH polarization using MLR (**a**) or RF (**b**) statistical algorithm. The gray dots represent the estimates obtained on the training subset, while the black dots come from the validation subset.

4.1.2. Multi-Incidence and Multi-Polarization Estimates of C-Band Backscattering Coefficients

The results obtained in the C-band are presented in Figure 8, distinguishing the performance associated with each state of polarization. As in the previous section, the results obtained with MLR are based on variables with significant *p*-values. For signals acquired in co-polarization states (i.e., HH and VV), the estimates are based on the incidence angle and topsoil moisture, while for cross-polarization states, the following descriptors have *p*-values less than 0.05: the topsoil moisture, the fraction of clay, the standard deviation of roughness heights and the autocorrelation length collected in the direction parallel to the tillage orientation regarding the surface roughness. As previously mentioned, all the surface and satellite descriptors are considered for RF. Compared with the X-band results, the levels of accuracy are lower, with correlation values of 0.65/0.73, 0.65/0.71 and 0.58/0.70 for the two tested algorithms (i.e., MLR/RF) and for the HH, VV and VH polarizations, respectively (focusing on validation performance). The estimates are characterized by a near-zero bias, regardless of the considered configuration. Statistical models associated with co-polarizations (i.e., HH and VV) have similar levels of error, with RMSE values between 1.53 and 1.75 dB (Figure 8a–d). The error is slightly higher with cross-polarization (VH), with values of 2.22 dB for MLR (Figure 8e) and 1.95 dB for RF (Figure 8f) (comparable results are obtained with HV polarization, not shown here). Moreover, the RF algorithm provides results with higher stability, as evidenced by the quasi-similar levels of the statistical indices between the training and validation phases, while the performance is slightly degraded with MLR. Such behaviors have already been pointed out in previous studies [58,59], with RF algorithms being associated with high predictive ability (showing a high level of performance in the multifactorial context in modeling non-linear relationships) and results with high stability (a characteristic mainly explained by the bootstrap aggregating procedure). As previously stated for the X-band, the results obtained in the C-band in the HH polarization state can be compared with those obtained with semi-empirical models on the same dataset [30]. The performance associated with the initial models proposed by Oh et al. [11] and Oh [12] or Dubois et al. [10] is lower than that obtained with the two statistical algorithms, as evidenced by the values of correlation (between 0.31 and 0.44) or corresponding errors (between 2.27 and 3.66 dB). After the improvement procedure (taking into account biases with regard to surface descriptors), the accuracy of the semi-empirical models is close (r = 0.65, RMSE = 1.74 dB) to that obtained with MLR but remains lower than that obtained with RF (r = 0.73 and RMSE = 1.60 dB for RF).

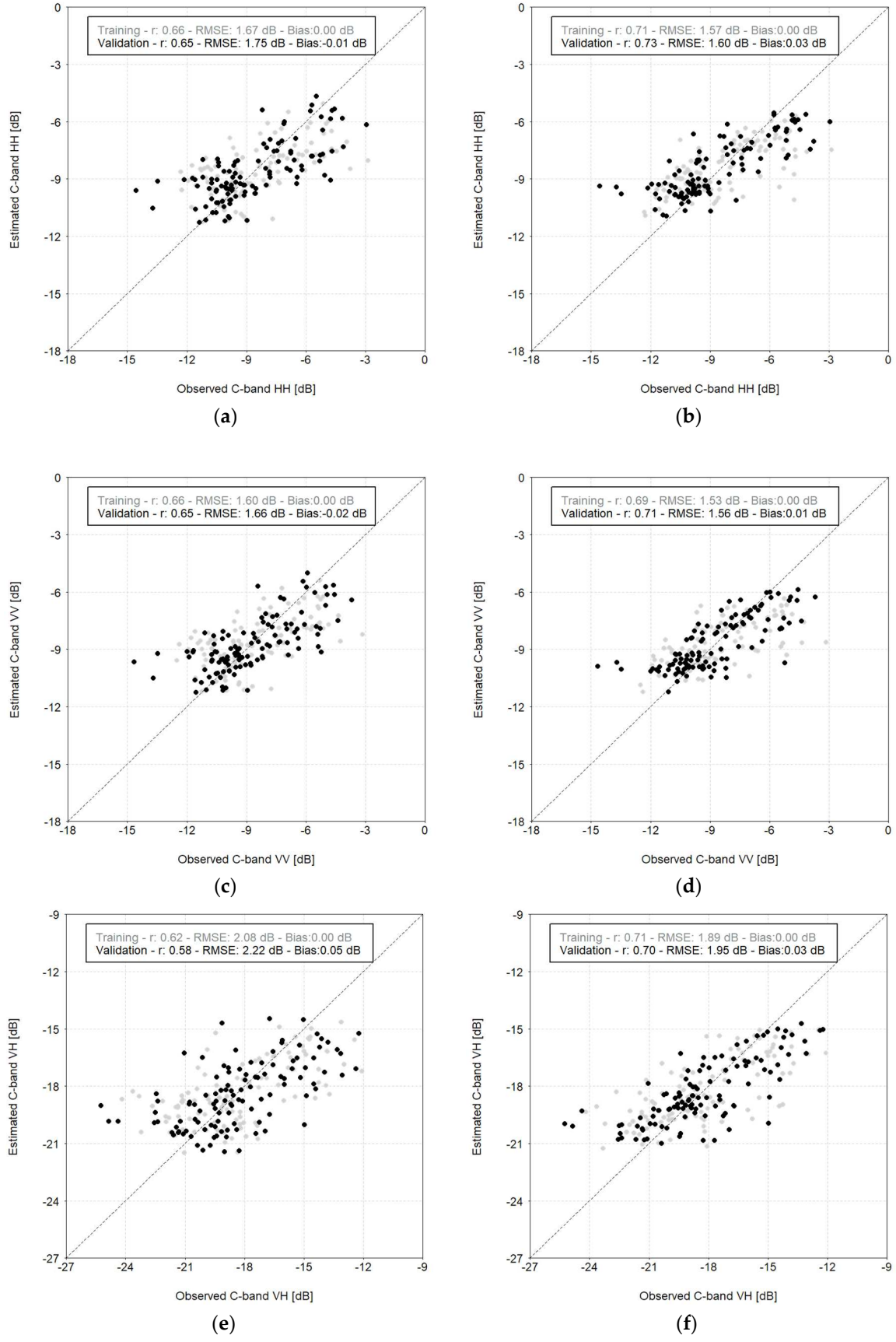

Figure 8. Comparison between simulated and observed backscattering coefficients in the C-band in three polarizations states (HH (**a**,**b**), VV (**c**,**d**) and VH (**e**,**f**)) using MLR (**left**) or RF (**right**) statistical algorithm. The gray dots represent the estimates obtained on the training subset, while the black dots come from the validation subset.

4.1.3. Evaluation of the Statistical Algorithms Compared to Models Developed in the Literature—Which Approach to Retain?

This section compares the performance obtained in this paper to that obtained in previous studies [24,29,30,60–63]. It focuses on statistical criteria (i.e., correlation coefficient and RMSE) obtained for satellite signals acquired in the X- and C-bands in HH, VV and VH polarization states (Figure 9). The studies used in the comparison of performance with the models developed in this work did not all use the same performance evaluation statistics. Indeed, some of them used only the correlation coefficient, while others used only the RMSE. Figure 9 summarizes the statistical performance obtained for each model used for the comparison (r and/or RMSE) for the four satellite configurations analyzed in the present study. It is important to note that these performance measures were obtained from the original datasets used to build the models, unlike the previous parts, where the models were evaluated on the dataset used in this study.

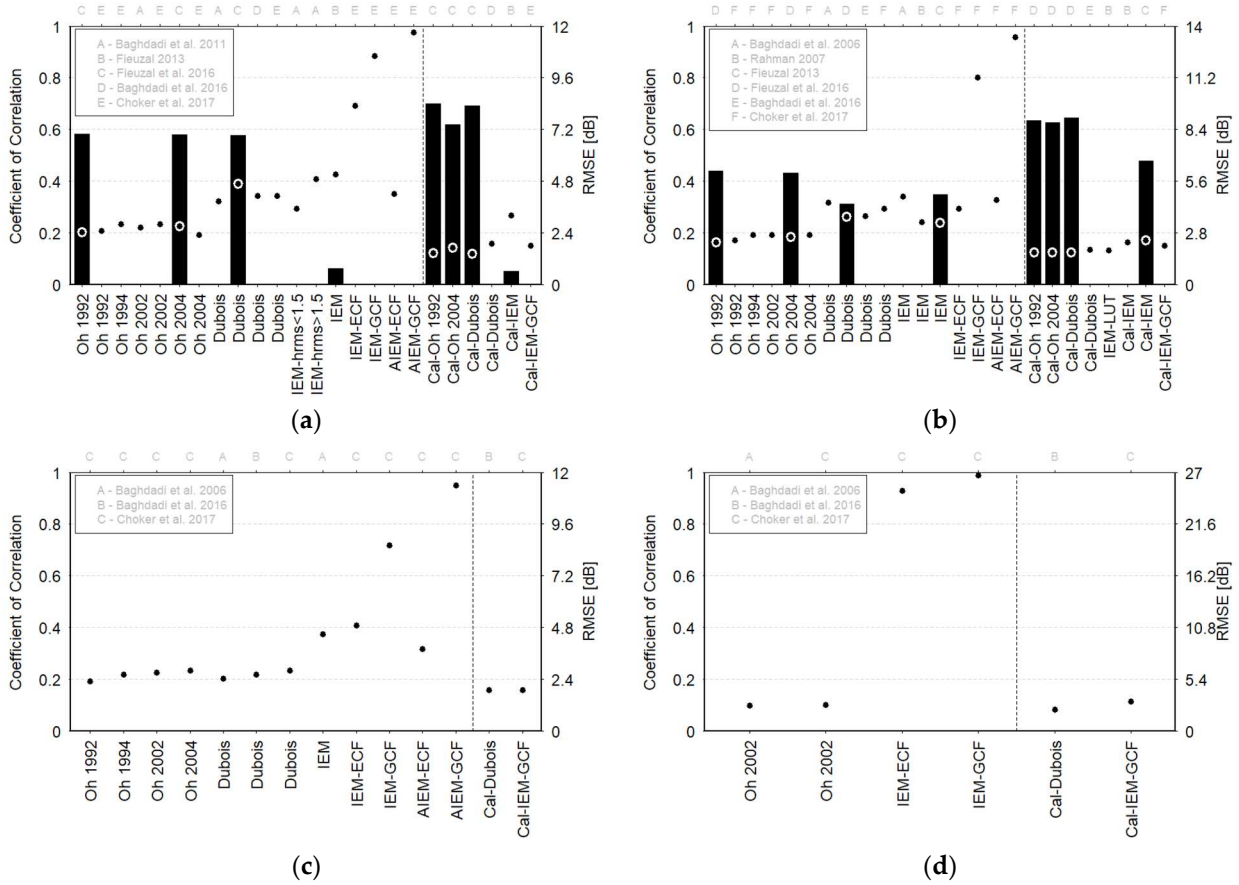

Figure 9. Statistical performance: RMSE (dots) and correlations (bars) obtained in previous studies by comparing the modeled and satellite-derived backscattering coefficients in the X-band in the HH polarization state (**a**) and in the C-band in HH, VV and VH polarizations states (**b**–**d**, respectively). In each figure, the vertical dotted line distinguishes the original models (on the left) from the modified versions of the models (on the right) [24,29,30,60–63].

Semi-empirical models tested on different study sites present error levels ranging from 2.3 to 4.7 dB in the X-band (and correlations close to 0.58) and from 2.3 to 4.4 dB in the C-band (and correlations between 0.31 and 0.44). The results of the signal estimations acquired with HH polarization show similarities, namely, lower error levels for the models proposed by Oh [11,12] compared to the performance associated with the Dubois model [10]. Concerning the other polarization states (i.e., VV or VH), fewer studies show error levels ranging from 2.4 to 2.8 dB. Physical approaches do not offer any improvement in the estimation of radar signals. Their performance appears limited, as evidenced by the error

levels in the X- and C-bands, with values from 3.5 to 11.7 dB and 3.3 to 26.7 dB, respectively, and correlations less than 0.35.

Given these results, in order to overcome the limitations displayed by these models, different approaches have been proposed, such as the semi-empirical calibration of the IEM model [25–28], the recalibration of the initial equations of the models or the reduction in different biases of semi-empirical models [24,29,30]. These changes are accompanied by a decrease in estimate dispersion, which is accompanied by a higher level of performance. The IEM model corrected for roughness bias has, for example, lower error levels in the X- or C-band (with values between 1.8 and 3.2 dB and between 1.9 and 3.1 dB, respectively). The same applies to approaches that aim at modifying semi-empirical models, with error levels in X- or C-band between 1.4 and 1.9 dB and between 1.7 and 2.2, respectively. Nevertheless, these approaches remain limited, and the levels of precision of the statistical approaches (presented in this study) exceed those obtained with semi-empirical (i.e., Oh's [11,12] and Dubois' [10] models, results presented in [30]) or physical (i.e., IEM [13], results presented in [24]) models implemented at the same study site (results presented in the two previous sections). This raises the question of the initial formalism of the models and the question of the representativeness/quality of the ground measurements. Indeed, models adjusted for different biases should have a performance at least equivalent to that of statistical approaches. At this stage, the modified models are in a deadlock, having extracted as much information as possible from the biases toward the input variables.

4.2. Importance of the Soil Descriptors and Incidence Angle in Backscattering Estimates

In the case of MLR, the models rely on a limited number of explanatory variables, especially in the case of signals acquired with co-polarization. For the X-band, incidence angles and TSM account for 59.2 and 40.8% of the explained variance, respectively. Regarding the C-band, the variance explained by TSM is more important, with 77.1 and 79.7% for HH and VV polarizations, respectively (the variance explained by the incidence angle is 22.9 and 20.3%, depending on the considered polarization). Finally, for the C-band in the cross-polarization state, the proportion of variance explained by TSM reaches 86.3%; the clay fraction, the standard deviation of roughness heights and the autocorrelation length collected in the direction parallel to the tillage orientation regarding the surface roughness account for 3.6, 8.5 and 1.6%, respectively.

The relative importance of the descriptors used as input variables of RF algorithms for the estimation of backscattering coefficients is presented in Figure 10. The general trends in the level of importance of the variables for the tested satellite configurations are relatively close (absolute levels are, however, specific to the considered frequency and polarization) and appear consistent with previous studies dealing with the analysis of microwave signals observed over bare agricultural soils.

Regardless of the microwave wavelength considered, the topsoil moisture is the most significant surface descriptor. The importance of this variable in the estimation of backscatter coefficients is the highest in the case of the C-band, with values ranging from 44.0 to 46.7% for the various polarizations (Figure 10). For the X-band, the importance level associated with surface moisture is 38.8%.

For the other variables, the order and level of importance vary with the considered satellite configuration. The effect of the incidence angle is the highest in the case of the X-band (importance of 39.9%, Figure 10), with a level close to that of the surface humidity (38.8%). This importance of the incidence angle is lower in the case of the C-band, with an average level close to 20% for co-polarizations. In the case of cross-polarization, the importance of the incidence angle is the lowest, exceeded by topsoil moisture, roughness and texture, whose levels reach 44.0, 27.7 and 18.0%, respectively. This difference between polarization states is consistent with various studies that show a low angular sensitivity in the case of signals acquired with cross-polarization [2,64–66]. Conversely, the large difference between signals acquired in the same polarization state (i.e., HH) in the X- and C-bands regarding the effect of the incidence angle should be interpreted with caution.

Indeed, images acquired in the X-band are mainly acquired at 27.3 and 53.3°, therefore displaying a maximum angular difference of ~26°. In the C-band, this difference is smaller (close to 16°), limiting the comparison of the importance of the incidence angle between signals acquired at different frequencies.

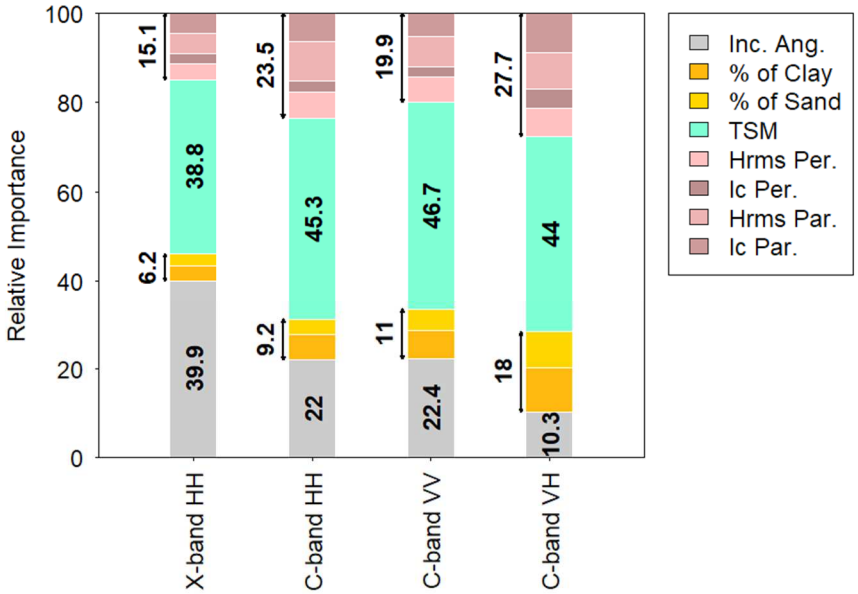

Figure 10. Comparison of the importance (expressed in percent) of the input parameters (incidence angle and soil descriptors) considering the RF algorithms in the X-band and C-band in the 3 polarizations states (HH, VV and VH).

The four components of roughness considered in the approach have a higher importance in the C-band, with levels of 23.5% for HH, 19.9% for VV and 27.7% for VH polarization, compared to 15.1% for the X-band (Figure 10, topmost values). This lower importance of roughness in signals acquired in the X-band is also highlighted in various other studies; the sensitivity to surface roughness thus increases with the considered wavelength [9,67]. Among the four components considered in this study, the levels of importance of h_{rms} are slightly higher than those associated with l_c (averages of 6.5 and 4.8%, respectively). Regardless of the considered satellite configuration, the two roughness variables derived from the profiles measured in the parallel direction are associated with levels of importance higher than those measured in the perpendicular direction (averages of 7.0 and 4.3%, respectively).

Finally, the texture components show limited importance, which reaches 18.0% in the case of the C-band with VH polarization. This level is lower for signals acquired with HH polarization, that is, 6.2% and 9.2% for the X- and C-bands, respectively. The values of importance associated with the clay content are higher (mean of 7.2%) than those of the sand content (5.3%), regardless of the satellite configuration considered. The moderate influence of texture on signals acquired in the X- and C-bands is thus consistent with the results presented in [68], with the effects of the fractions of sand, silt and clay being more pronounced on signals acquired at lower frequencies (e.g., in the L-band).

5. Conclusions

This study aimed at modeling the backscattering coefficients observed at the plot spatial scale with different viewing configurations (regarding the frequency, polarization and incidence angle) over bare agricultural surfaces. The two statistical algorithms developed in this study (i.e., multiple linear regression and random forest) present a higher magnitude of performance than those in previous studies (based on different modeling assumptions, that is, semi-empirical or physical), with higher accuracy in the X-band (correlation of 0.86 and RMSE of 1.03 dB) compared to that obtained with the different polarizations in

the C-band (correlations greater than 0.58 and RMSE less than 2.22 dB). These two models are not influenced in the same way by surface descriptors. In the linear approach, the information is mainly carried by the surface moisture and the angle of incidence (especially in the case of co-polarized signals, regardless of the frequency), while the influence of roughness or texture becomes significant for cross-polarized signals in the C-band. On the contrary, all the surface descriptors contribute information in the approach based on RF, with the algorithm giving access to more complex relations. Overall, the RF algorithm is the most robust and reliable for simulating all radar configurations (from the band and polarization perspectives). Both surpass the performance presented in previous studies based on either empirical, semi-empirical or physical models.

The analyses carried out in this study highlight the importance of topsoil moisture in the dynamics of backscattering coefficients, opening the way to a new perspective on its estimation from SAR images.

Supplementary Materials: Random Forest modeling was performed using R software. For each of the tested configurations, the trained models are available on request from the authors. They can also be downloaded at https://www.mdpi.com/article/10.3390/app13084893/s1, where a sample formatted data matrix of the input file and an RDS file per configuration are available.

Author Contributions: R.F. and F.B. contributed to the data collection, conceptualization, analysis of the results, and writing of the manuscript. All authors have read and agreed to the published version of the manuscript.

Funding: This research received no external funding.

Institutional Review Board Statement: Not applicable.

Informed Consent Statement: Not applicable.

Data Availability Statement: The data presented in this study are available on request from the corresponding author.

Acknowledgments: The authors wish to thank the DLR (German Space Agency), SOAR Project, and CNES (Centre National des Etudes Spatiales) for their support, funding, and satellite images (proposals HYD0611 and SOAR-EU and Categorie-1 ESA project no. 6843). In addition, the authors wish to thank the farmers (Blanquet, Bollati, Brardo, Pavan, and Peres) for their time and valuable discussions and the people who helped to collect the ground data.

Conflicts of Interest: The authors declare no conflict of interest.

Appendix A

The values of the multiple linear regression parameters are listed in Table A1 for the analyzed satellite configurations.

Table A1. Summary of the values of multiple linear regression parameters for relationships obtained in the X-band in the HH polarization state and in the C-band in HH and VV polarization states considering the incidence angle and the topsoil moisture.

Band	Polar. States	Inc. Ang.	TSM	Cte
X	HH	−0.100	11.025	−7.220
C	HH	−0.163	15.941	−6.030
C	VV	−0.147	15.372	−6.575

The backscattering coefficients can be estimated using Equation (A1) and the parameters corresponding to the chosen satellite configuration.

$$\sigma^{\circ} Freq_{Pol} = X_1 \times P_{Inc.Ang.} + X_2 \times P_{TSM} + Cte, \quad \text{(A1)}$$

where *Freq* is the considered band, *Pol* is the polarization state, X_1 is the incidence angle, X_2 is *TSM*, and *P* is the corresponding parameter.

Table A2. Summary of the values of the multiple linear regression parameters for relationships obtained in the C-band in HV and VH polarization states considering the topsoil moisture, the fraction of clay, the standard deviation of roughness heights and the autocorrelation length collected in the direction parallel to the tillage orientation regarding the surface roughness.

Band	Polar. States	TSM	% of Clay	H_{rms} Par.
X	HH	−0.100	11.025	−7.220
C	HH	−0.163	15.941	−6.030
C	HV	20.215	−8.211	0.742

The backscattering coefficients can be estimated using Equation (A2) and the parameters corresponding to the chosen satellite configuration.

$$\sigma^{\circ} Freq_{Pol} = X_1 \times P_{TSM} + X_2 \times P_{\%\ of\ Clay} + X_3 \times P_{Hrms\ Par.} + X_4 \times P_{lc\ Par.} + Cte, \quad \text{(A2)}$$

where *Freq* is the considered band, *Pol* is the polarization state, X_1 is TSM, X_2 is the fraction of clay, X_3 and X_4 are the standard deviation of roughness heights and the autocorrelation length, both collected in the direction parallel to the tillage orientation regarding the surface roughness, and *P* is the corresponding parameter.

References

1. Brown, S.C.M.; Quegan, S.; Morrison, K.; Bennett, J.C.; Cookmartin, G. High-resolution measurements of scattering in wheat canopies-implications for crop parameter retrieval. *IEEE Trans. Geosci. Remote Sens.* **2003**, *41*, 1602–1610. [CrossRef]
2. Fieuzal, R.; Baup, F.; Marais-Sicre, C. Monitoring wheat and rapeseed by using synchronous optical and radar satellite data—from temporal signatures to crop parameters estimation. *Adv. Remote Sens.* **2013**, *2*, 162–180. [CrossRef]
3. Picard, G.; Le Toan, T.; Mattia, F. Understanding C-band radar backscatter from wheat canopy using a multiple-scattering coherent model. *IEEE Trans. Geosci. Remote Sens.* **2003**, *41*, 1583–1591. [CrossRef]
4. Saich, P.; Borgeaud, M. Interpreting ERS SAR signatures of agricultural crops in Flevoland, 1993–1996. *IEEE Trans. Geosci. Remote Sens.* **2000**, *38*, 651–657. [CrossRef]
5. Aubert, M.; Baghdadi, N.; Zribi, M.; Douaoui, A.; Loumagne, C.; Baup, F.; El Hajj, M.; Garrigues, S. Analysis of TerraSAR-X data sensitivity to bare soil moisture, roughness, composition and soil crust. *Remote Sens. Environ.* **2011**, *115*, 1801–1810. [CrossRef]
6. Champion, I.; Faivre, R. Sensitivity of the radar signal to soil moisture: Variation with incidence angle, frequency, and polarization. *IEEE Trans. Geosci. Remote Sens.* **1997**, *35*, 781–783. [CrossRef]
7. Dobson, M.C.; Ulaby, F.T. Microwave backscatter dependence on surface roughness, soil moisture, and soil texture: Part III—Soil tension. *IEEE Trans. Geosci. Remote Sens.* **1981**, *19*, 51–61. [CrossRef]
8. Mattia, F.; Le Toan, T.; Souyris, J.C.; De Carolis, G.; Floury, N.; Posa, F.; Pasquariello, G. The effect of surface roughness on multifrequency polarimetric SAR data. *IEEE Trans. Geosci. Remote Sens.* **1997**, *35*, 954–966. [CrossRef]
9. Ulaby, F.T.; Batlivala, P.P.; Dobson, M.C. Microwave backscatter dependence on surface roughness, soil moisture, and soil texture: Part I—Bare Soil. *IEEE Trans. Geosci. Electron.* **1978**, *16*, 286–295. [CrossRef]
10. Dubois, P.C.; van Zyl, J.; Engman, T. Measuring soil moisture with imaging radars. *IEEE Trans. Geosci. Remote Sens.* **1995**, *33*, 915–926. [CrossRef]
11. Oh, Y.; Sarabandi, K.; Ulaby, F.T. An empirical model and an inversion technique for radar scattering from bare soil surfaces. *IEEE Trans. Geosci. Remote Sens.* **1992**, *30*, 370–381. [CrossRef]
12. Oh, Y. Quantitative retrieval of soil moisture content and surface roughness from multipolarized radar observations of bare soil surfaces. *IEEE Geosci. Remote Sens.* **2004**, *42*, 596–601. [CrossRef]
13. Chen, K.S.; Wu, T.D.; Tsay, M.K.; Fung, A.K. A note on the multiple scattering in an IEM model. *IEEE Trans. Geosci. Remote Sens.* **2000**, *38*, 249–256. [CrossRef]
14. Fung, A.K.; Li, Z.; Chen, K.S. Backscattering from a randomly rough dielectric surface. *IEEE Trans. Geosci. Remote Sens.* **1992**, *30*, 356–369. [CrossRef]
15. Fung, A.K. *Microwave Scattering and Emission Models and Their Applications*; Artech House Publishers: Norwood, MA, USA, 1994.
16. Hasting, F.D.; Schneider, J.B.; Broschat, S.L. A Monte Carlo FDTD technique for rough surface scattering. *IEEE Trans. Antennas Propag.* **1995**, *43*, 1183–1191. [CrossRef]
17. Soriano, G.; Saillard, M. Scattering of electomagnetic waves from two dimensional rough surfaces with impedance approximation. *J. Opt. Soc. Am.* **2001**, *18*, 124–133. [CrossRef] [PubMed]
18. Ulaby, F.T.; Moore, R.K.; Fung, A.K. Microwave Remote Sensing: Active and Passive. In *Radar Remote Sensing and Surface Scattering and Emission Theory*; Artech House Publishers: Norwood, MA, USA, 1982; Volume II.
19. Johnson, J.T.; Warnick, K.F.; Xu, P. On the geometrical optics (Hagfors' law) and physical optics approximations for scattering from exponentially correlated surfaces. *IEEE Trans. Geosci. Remote Sens.* **2007**, *45*, 2619–2629. [CrossRef]

20. Imperatore, P.; Iodice, A.; Riccio, D. Electromagnetic wave scattering from layered structures with an arbitrary number of rough interfaces. *IEEE Trans. Geosci. Remote Sens.* **2009**, *47*, 1056–1072. [CrossRef]
21. Iodice, A.; Natale, A.; Riccio, D. Kirchhoff scattering from fractal and classical rough surfaces: Physical interpretation. *IEEE Trans. Ant. Prop.* **2013**, *61*, 2156–2163. [CrossRef]
22. Comite, D.; Pierdicca, N. Monostatic and bistatic scattering modeling of the anisotropic rough soil. *IEEE Trans. Geosci. Remote Sens.* **2019**, *57*, 2543–2556. [CrossRef]
23. Di Martino, G.; Di Simone, A.; Iodice, A.; Riccio, D. Bistatic scattering from anisotropic rough surfaces via a closed-form two-scale model. *IEEE Trans. Geosci. Remote Sens.* **2021**, *59*, 3656–3671. [CrossRef]
24. Fieuzal, R. *Apports des Données Radar Pour L'estimation des Paramètres Biophysiques des Surfaces Agricoles*; Sciences de la Terre; Université Toulouse III-Paul Sabatier: Toulouse, France, 2013.
25. Baghdadi, N.; King, C.; Chanzy, A.; Wigneron, J.P. An empirical calibration of the integral equation model based on SAR data, soil moisture and surface roughness measurement over bare soils. *Int. J. Remote Sens.* **2002**, *23*, 4325–4340. [CrossRef]
26. Baghdadi, N.; Gherboudj, I.; Zribi, M.; Sahebi, M.; King, C.; Bonn, F. Semi-empirical calibration of the IEM backscattering model using radar images and moisture and roughness field measurements. *Int. J. Remote Sens.* **2004**, *25*, 3593–3623. [CrossRef]
27. Baghdadi, N.; Holah, N.; Zribi, M. Calibration of the Integral Equation Model for SAR data in C-band and HH and VV polarizations. *Int. J. Remote Sens.* **2006**, *27*, 805–816. [CrossRef]
28. Baghdadi, N.; Chaaya, J.A.; Zribi, M. Semiempirical calibration of the integral equation model for SAR data in C-band and cross polarization using radar images and field measurements. *IEEE Geosci. Remote Sens. Lett.* **2011**, *8*, 14–18. [CrossRef]
29. Baghdadi, N.; Choker, M.; Zribi, M.; Hajj, M.E.; Paloscia, S.; Verhoest, N.E.C.; Lievens, H.; Baup, F.; Mattia, F. A new empirical model for radar scattering from bare soil surfaces. *Remote Sens.* **2016**, *8*, 920. [CrossRef]
30. Fieuzal, R.; Baup, F. Improvement of bare soil semiempirical radar backscattering models (Oh and Dubois) with SAR multi-spectral satellite data (at X, C and L bands). *Adv. Remote Sens.* **2016**, *5*, 296–314. [CrossRef]
31. Callens, M.; Verhoest, N.E.C.; Davidson, M.W.J. Parameterization of tillage-induced single-scale soil roughness from 4-M profiles. *IEEE Trans. Geosci. Remote Sens.* **2006**, *44*, 878–888. [CrossRef]
32. Davidson, M.W.J.; Le Toan, T.; Mattia, F.; Satalino, G.; Manninen, T.; Borgeaud, M. On the characterization of agricultural soil roughness for radar remote sensing studies. *IEEE Trans. Geosci. Remote Sens.* **2000**, *38*, 630–640. [CrossRef]
33. Jackson, T.J.; McNairn, H.; Weltz, M.A.; Brisco, B.; Brown, R. First order surface roughness correction of active microwave observations for estimating soil moisture. *IEEE Trans. Geosci. Remote Sens.* **1997**, *35*, 1065–1069. [CrossRef]
34. Du, P.; Samat, A.; Waske, B.; Liu, S.; Li, Z. Random Forest and Rotation Forest for fully polarized SAR image classification using polarimetric and spatial features. *ISPRS J. Photogramm. Remote. Sens.* **2015**, *105*, 38–53. [CrossRef]
35. Loosvelt, L.; Peters, J.; Skriver, H.; Lievens, H.; Van Coillie, F.M.B.; De Baets, B.; Verhoest, N.E.C. Random Forests as a tool for estimating uncertainty at pixel-level in SAR image classification. *Int. J. Appl. Earth Obs. Geoinf.* **2012**, *19*, 173–184. [CrossRef]
36. Marais Sicre, C.; Fieuzal, R.; Baup, F. Contribution of multispectral (optical and radar) satellite images to the classification of agricultural surfaces. *Int. J. Appl. Earth Obs. Geoinf.* **2020**, *84*, 101972. [CrossRef]
37. Waske, B.; Braun, M. Classifier ensembles for land cover mapping using multitemporal SAR imagery. *ISPRS J. Photogramm. Remote. Sens.* **2009**, *64*, 450–457. [CrossRef]
38. Baghdadi, N.; Cresson, R.; El Hajj, M.; Ludwig, R.; La Jeunesse, I. Estimation of soil parameters over bare agriculture areas from C-band polarimetric SAR data using neural networks. *Hydrol. Earth Syst. Sci.* **2012**, *16*, 1607–1621. [CrossRef]
39. Bai, X.; He, B.; Li, X.; Zeng, J.; Wang, X.; Wang, Z.; Zeng, Y.; Su, Z. First Assessment of Sentinel-1A data for surface soil moisture estimations using a coupled water cloud model and advanced integral equation model over the Tibetan plateau. *Remote Sens.* **2017**, *9*, 714. [CrossRef]
40. El Hajj, M.; Baghdadi, N.; Zribi, M.; Bazzi, H. Synergic use of Sentinel-1 and Sentinel-2 images for operational soil moisture mapping at high spatial resolution over agricultural areas. *Remote Sens.* **2017**, *9*, 1292. [CrossRef]
41. Paloscia, S.; Pettinato, S.; Santi, E.; Notarnicola, C.; Pasolli, L.; Reppucci, A. Soil moisture mapping using Sentinel-1 images: Algorithm and preliminary validation. *Remote Sens. Environ.* **2013**, *134*, 234–248. [CrossRef]
42. Santi, E.; Paloscia, S.; Pettinato, S.; Notarnicola, C.; Pasolli, L.; Pistocchi, A. Comparison between SAR soil moisture estimates and hydrological model simulations over the Scrivia test site. *Remote Sens.* **2013**, *5*, 4961–4976. [CrossRef]
43. Santi, E.; Paloscia, S.; Pettinato, S.; Fontanelli, G. Application of artificial neural networks for the soil moisture retrieval from active and passive microwave spaceborne sensors. *Int. J. Appl. Earth Obs. Geoinf.* **2016**, *48*, 61–73. [CrossRef]
44. Baghdadi, N.; El Hajj, M.; Choker, M.; Zribi, M.; Bazzi, H.; Vaudour, E.; Gilliot, J.M.; Ebengo, D.M. Potential of Sentinel-1 images for estimating the soil roughness over bare agricultural soils. *Water* **2018**, *10*, 131. [CrossRef]
45. Maleki, M.; Amini, J.; Notarnicola, C. Soil roughness retrieval from TerraSar-X data using neural network and fractal method. *Adv. Space Res.* **2019**, *64*, 1117–1129. [CrossRef]
46. Zribi, M.; Kotti, F.; Lili-Chabaane, Z.; Baghdadi, N.; Ben Issa, N.; Amri, R.; Amri, B.; Chehbouni, A. Soil texture estimation over a semiarid area using TerraSAR-X radar data. *IEEE Trans. Geosci. Remote Sens. Lett.* **2012**, *9*, 353–357. [CrossRef]
47. Ezzahar, J.; Ouaadi, N.; Zribi, M.; Elfarkh, J.; Aouade, G.; Khabba, S.; Er-Raki, S.; Chehbouni, A.; Jarlan, L. Evaluation of backscattering models and support vector machine for the retrieval of bare soil moisture from Sentinel-1 data. *Remote Sens.* **2020**, *12*, 72. [CrossRef]

48. Fieuzal, R.; Baup, F. Use of statistical approach combined with SAR polarimetric indices for surface moisture estimation over bare agricultural soil. *Environ. Sci. Proc.* **2021**, *5*, 22.
49. Fieuzal, R.; Baup, F. Estimation of surface soil moisture at the intra-plot spatial scale by using low and high incidence angles TerraSAR-X images. *Environ. Sci. Proc.* **2021**, *5*, 6.
50. Pasolli, L.; Notarnicola, C.; Bruzzone, L.; Bertoldi, G.; Chiesa, S.D.; Niedrist, G.; Tappeiner, U.; Zebisch, M. Polarimetric RADARSAT-2 imagery for soil moisture retrieval in alpine areas. *Can. J. Remote Sens.* **2011**, *37*, 535–547. [CrossRef]
51. Fieuzal, R.; Baup, F. Statistical estimation of backscattering coefficients in X-band over bare agricultural soils. In Proceedings of the 2020 Mediterranean and Middle-East Geoscience and Remote Sensing Symposium (M2GARSS), Tunis, Tunisia, 9–11 March 2020; pp. 302–305.
52. Baup, F.; Fieuzal, R.; Marais-Sicre, C.; Dejoux, J.F.; le Dantec, V.; Mordelet, P.; Claverie, M.; Hagolle, O.; Lopes, A.; Keravec, P.; et al. MCM'10: An experiment for satellite multi-sensors crop monitoring from high to low resolution observations. In Proceedings of the 2012 IEEE International Geoscience and Remote Sensing Symposium, Munich, Germany, 22–27 July 2012; pp. 4849–4852.
53. Breit, H.; Fritz, T.; Balss, U.; Lachaise, M.; Niedermeier, A.; Vonavka, M. TerraSAR-X SAR processing and products geoscience and remote sensing. *IEEE Trans. Geosci. Remote Sens.* **2010**, *48*, 727–740. [CrossRef]
54. Morena, L.C.; James, K.V.; Beck, J. An introduction to the RADARSAT-2 mission. *Can. J. Remote Sens.* **2004**, *30*, 221–234. [CrossRef]
55. NEST. Available online: http://nest.array.ca/web/nest (accessed on 26 November 2015).
56. Breiman, L. Random Forests. *Mach. Learn.* **2001**, *45*, 5–32. [CrossRef]
57. Grömping, U. Variable importance assessment in regression: Linear regression versus random forest. *Am. Statistician.* **2009**, *63*, 308–319. [CrossRef]
58. Belgiu, M.; Drăguţ, L. Random Forest in remote sensing: A review of applications and future directions. *ISPRS J. Photogramm. Remote. Sens.* **2016**, *114*, 24–31. [CrossRef]
59. Fawagreh, K.; Gaber, M.M.; Elyan, E. Random forests: From early developments to recent advancements. *Syst. Sci. Control Eng.* **2014**, *2*, 602–609. [CrossRef]
60. Baghdadi, N.; Zribi, M. Evaluation of radar backscatter models IEM, OH and Dubois using experimental observations. *Int. J. Remote Sens.* **2006**, *27*, 3831–3852. [CrossRef]
61. Baghdadi, N.; Saba, E.; Aubert, M.; Zribi, M.; Baup, F. Evaluation of radar backscattering models IEM, Oh, and Dubois for SAR data in X-Band over bare soils. *IEEE Geosci. Remote Sens. Lett.* **2011**, *8*, 1160–1164. [CrossRef]
62. Choker, M.; Baghdadi, N.; Zribi, M.; El Hajj, M.; Paloscia, S.; Verhoest, N.E.C.; Lievens, H.; Mattia, F. Evaluation of the Oh, Dubois and IEM backscatter models using a large dataset of SAR data and experimental soil measurements. *Water* **2017**, *9*, 38. [CrossRef]
63. Rahman, M.M.; Moran, M.S.; Thoma, D.P.; Bryant, R.; Sano, E.E.; Holifield Collins, C.D.; Skirvin, S.; Kershner, C.; Orr, B.J. A derivation of roughness correlation length for parameterizing radar backscatter models. *Int. J. Remote Sens.* **2007**, *28*, 3995–4012. [CrossRef]
64. Fieuzal, R.; Baup, F. Estimation of leaf area index and crop height of sunflowers using multi-temporal optical and SAR satellite data. *Int. J. Remote Sens.* **2016**, *37*, 2780–2809. [CrossRef]
65. Ulaby, F.T. Radar Response to Vegetation. *IEEE Trans. Ant. Propag.* **1975**, *23*, 36–45. [CrossRef]
66. Ulaby, F.T.; Bradley, G.A.; Dobson, M.C. Microwave backscatter dependence on surface roughness, soil moisture, and soil texture: Part II—Vegetation-covered soil. *IEEE Trans. Geosci. Electron.* **1970**, *17*, 33–40. [CrossRef]
67. Brisco, B.; Brown, R.J.; Snider, B.; Sofko, G.J.; Koehler, J.A.; Wacker, A.G. Tillage effects on the radar backscattering coefficient of grain stubble fields. *Int. J. Remote Sens.* **1991**, *12*, 2283–2298. [CrossRef]
68. Hallikainen, M.T.; Ulaby, F.T.; Dobson, M.C.; El-Rayes, M.A.; Lil-Kun, W. Microwave dielectric behavior of wet soil—Part 1: Empirical models and experimental observations. *IEEE Trans. Geosci. Remote Sens.* **1985**, *23*, 25–34. [CrossRef]